Inorg. Chem. **2009**, *48*, 2944−2955

Zn and Fe Complexes Containing a Redox Active Macrocyclic Biquinazoline Ligand

Priyabrata Banerjee, Anna Company, Thomas Weyhermüller, Eckhard Bill, and Corinna R. Hess*

Max Planck Institut für Bioanorganische Chemie, Stiftstrasse 34-36, D-45470 Mülheim an der Ruhr, Germany, and Departament de Química, Universitat de Girona, Campus de Montilivi s/n, E-17071 Girona, Spain

Received October 21, 2008

A series of iron and zinc complexes has been synthesized, coordinated by the macrocyclic biquinazoline ligand, 2-4:6-8-bis(3,3,4,4-tetramethyldihydropyrrolo)-10-15-(2,2′-biquinazolino)-[15]-1,3,5,8,10,14-hexaene-1,3,7,9,11,14-N_6 (Mabiq). The Mabiq ligand consists of a bipyrimidine moiety and two dihydropyrrole units. The electronic structures of the metal-Mabiq complexes have been characterized using spectroscopic and density-functional theory (DFT) computational methods. The parent zinc complex exhibits a ligand-centered reduction to generate the metal-coordinated Mabiq radical dianion, establishing the redox non-innocence of this ligand. Iron-Mabiq complexes have been isolated in three oxidation states. This redox series includes low-spin ferric and low-spin ferrous species, as well as an intermediate-spin Fe^{II} compound. In the latter complex, the iron ion is antiferromagnetically coupled to a Mabiq-centered π-radical. The results demonstrate the rich redox chemistry and electronic properties of metal complexes coordinated by the Mabiq ligand.

Introduction

The prevalence and unique chemistry of porphyrin-containing proteins has spawned extensive research into synthetic analogues of this vital cofactor.[1,2] Heme enzymes, in particular, display a wide range of reactivity toward small molecules, including CO, NO, and O_2, as well as toward inert hydrocarbons.[3] Dioxygen and C−H activation by these enzymes especially have motivated the design of iron-containing N_4-macrocyclic complexes for catalysis.[4] The versatility of heme enzymes can be attributed partly to the numerous redox states available to the metalloporphyrin. Akin to their biological counterparts, a rich metal redox chemistry is associated with synthetic Fe-porphyrin and -corrole complexes, where oxidation states ranging from low-valent Fe^0 to Fe^V have been reported.[5,6] Slight modifications to the macrocyclic ligands often result in altered stabilities of the metal valence and spin state. For example, Fe^{IV}-porphyrins tend to be highly reactive, whereas high-valent iron states are readily stabilized by corroles.[7−9] The tetrapyrrole molecules display a range of oxidation states even in the absence of the metal center,[1,10] and the redox participation of these ligands is implicated in the catalytic cycles of heme enzymes.[11]

We have synthesized metal complexes containing the N_4-macrocyclic biquinazoline ligand, H(Mabiq) (Scheme 1), originally reported by von Zelewsky.[12] The Mabiq monoanion resembles the phthalocyanine and corrin family of ligands. However, the macrocycle contains only two pyrrole

* To whom correspondence should be addressed. E-mail: hess@mpi-muelheim.mpg.de. Phone: +49 208 306 3666.

(1) *The Porphyrin Handbook*, Kadish, K. M., Smith, K. M., Guilard, R., Eds.; Academic Press: New York, 2000; Vol. *1*.
(2) *The Porphyrin Handbook*, Kadish, K. M., Smith, K. M., Guilard, R., Eds.; Academic Press: New York, 2000; Vol. *2*.
(3) *The Porphyrin Handbook*, Kadish, K. M., Smith, K. M., Guilard, R., Eds.; Academic Press: New York, 2000; Vol. *4*.
(4) McLain, J. L.; Lee, J.; Groves, J. T. In *Biomimetic Oxidations Catalyzed by Transition Metal Complexes*; Meunier, B., Ed.; Imperial College Press: London, 2000, pp 91−169.
(5) Mashiko, T.; Reed, C. A.; Haller, K. J.; Scheidt, W. R. *Inorg. Chem.* **1984**, *23*, 3192.
(6) Groves, J. T. *J. Inorg. Biochem.* **2006**, *100*, 434.
(7) Simkhovich, L.; Galili, N.; Saltsman, I.; Goldberg, I.; Gross, Z. *Inorg. Chem.* **2000**, *39*, 2704.
(8) Vogel, E.; Will, S.; Tilling, A. S.; Neumann, L.; Lex, J.; Bill, E.; Trautwein, A. X.; Wieghardt, K. *Angew. Chem., Int. Ed. Engl.* **1994**, *33*, 731.
(9) *The Porphyrin Handbook*, Kadish, K. M., Smith, K. M., Guilard, R., Eds.; Academic Press: New York, 2000; Vol. *3*.
(10) Floriani, C.; Floriani-Moro, R. In *Inorganic, Organometallic and Coordination Chemistry*; Kadish, K. M., Smith, K. M., Guilard, R., Eds.; Academic Press: New York, 2000; Vol. *3*, pp 405−421.
(11) Sono, M.; Roach, M. P.; Coulter, E. D.; Dawson, J. H. *Chem. Rev.* **1996**, *96*, 2841.

10.1021/ic8020172 CCC: $40.75
Published on Web 02/25/2009

Scheme 1. Structure of the Deprotonated Monoanionic Mabiq Ligand

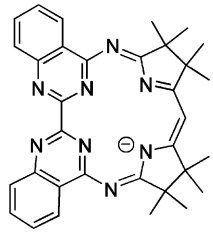

elements, while the opposing half of the ring is composed of pyrimidine units. The inherent redox non-innocence of two basic building blocks of this complex, the pyrrole and diimine elements, has been established previously.[13] Thus, the asymmetry and composition of this macrocycle suggested a unique redox chemistry for metal-Mabiq complexes. In addition, the outlying pair of bipyrimidine nitrogen donor atoms could potentially allow us to couple the electronic and redox properties of the macrocycle-bound metal to a second metal center.

As part of ongoing studies into the reactivity of metal-Mabiq complexes, we have synthesized a series of Fe and Zn complexes coordinated by this ligand (Scheme 2). The electronic structure of the various oxidation states of these compounds has been characterized using spectroscopic and density-functional theory (DFT) computational methods. Our studies confirm the redox non-innocence of the Mabiq ligand, which is readily reduced at the diketiminate moiety. Both ferric and ferrous Mabiq complexes have been isolated. The fully reduced iron complex provides one of a few examples of an intermediate-spin Fe^{II} complex, and exhibits strong antiferromagnetic coupling to a reduced Mabiq radical.

Results

Synthesis and Characterization. Zn-Mabiq Compounds. The diamagnetic [Zn^{II}(Mabiq)Cl] complex (**1**) was obtained from the reaction of H(Mabiq)[14] with 1 equiv of NEt_3 and $ZnCl_2$ in dichloromethane. The ^1H NMR of **1** (Supporting Information, Figure S1) shows a slight upfield shift in the aromatic protons and of the C−H proton of the diketiminate-backbone compared with the spectrum of the free ligand. The signal for the acidic cavity N−H proton of the free ligand, at 13.7 ppm, disappears upon coordination of the Zn ion. Four peaks in the region from 1.2−1.6 ppm correspond to the methyl protons of the dihydropyrrole backbone: the presence of the chloride ion on one face of the molecule leads to the inequivalence of these methyl protons. The coordination of Zn^{II} to the macrocyclic biquinazoline ligand results in a dramatic change in the electronic spectrum compared to that of H(Mabiq) (Figure 1). The Zn^{II} complex displays strong absorption bands at 372 and 502 nm, giving rise to the bright orange color of this compound in solution. These new absorption features cannot be ascribed merely to deprotonation of the diketiminate nitrogen, as previously stated,[12] since the addition of NEt_3 or *t*-BuOK to solutions of H(Mabiq) produces a spectrum identical to that of the protonated Mabiq molecule (Supporting Information, Figure S3).

The [Zn^{II}(Mabiq)Cl] complex can be one-electron reduced with a stoichiometric amount of sodium, which affords a green solution of [Zn^{II}(Mabiq)] (**2**) in tetrahydrofuran (THF). Addition of diethylether to a concentrated solution of **2** in THF leads to the precipitation of the green microcrystalline product. Elemental analysis and mass spectrometry specify the loss of the chloride ligand upon reduction. As signified by the color, the electronic spectrum of **2** exhibits new absorption features in the 600−800 nm region (Figure 1) that are not present in the UV−vis spectrum of **1**.

Fe-Mabiq Compounds. The Fe^{II}-coordinated Mabiq complex could not be synthesized according to the procedures decribed for **1**, using $FeCl_2$ as the starting material. Instead, the reaction in dichloromethane yields the oxidized [Fe^{III}(Mabiq)Cl_2] (**3**) as the primary product, even in the absence of air. Formation of the Fe^{III} complex presumably occurs via reduction of the solvent, as commonly observed in the synthesis of Fe-porphyrins and -corroles.[7,15] We have not made any attempts to characterize additional products of this reaction.[16] The crystalline, red [Fe^{III}(Mabiq)Cl_2] complex was subsequently isolated upon recrystallization of the crude reaction product from CH_2Cl_2/diethylether. The electronic spectrum of **3** displays multiple features in the visible region, as shown in Figure 2.

The Fe^{II} complex proved to be a much greater synthetic challenge. Further attempts to generate the divalent Fe-Mabiq complex avoided the use of halogen-containing reagents. The synthesis proceeds more cleanly using $Fe(OAc)_2$ as the source of iron. Reaction mixtures containing H(Mabiq) and a slight excess of $Fe(OAc)_2$ in acetonitrile turn dark green after several hours of stirring. We have tentatively assigned the product of this reaction as [Fe(Mabiq)(MeCN)(OAc)] (**4a**) since the coordination of the acetate group is likely. Attempts to crystallize this product were unsuccessful. The mass spectrum (ES-MS) of **4a** in MeCN shows two peaks with $m/z = 656$ and 597, which correlate with the loss of an acetonitrile ([M − MeCN + H]$^+$) and an acetate ligand ([656 − OAc]$^+$), respectively, from the proposed complex. The green solid obtained from the reaction mixtures is diamagnetic, as confirmed by NMR. The electronic spectrum of **4a** exhibits absorption bands at $\lambda_{max} = 354$, 440, 465, 620, and 660 nm.

(12) Mueller, E.; Bernardinelli, G.; von Zelewsky, A. *Inorg. Chem.* **1988**, *27*, 4545.
(13) Lu, C. C.; Bill, E.; Weyhermüller, T.; Bothe, E.; Wieghardt, K. *Inorg. Chem.* **2007**, *46*, 7880.
(14) H(Mabiq) is used to refer to the neutrally charged protonated macrocyclic biquinazoline complex, and (Mabiq) in the context of a metal complex (as in [Zn(Mabiq)Cl]) refers to the deprotonated monoanionic ligand.
(15) Bachmann, J.; Nocera, D. G. *J. Am. Chem. Soc.* **2005**, *127*, 4730.
(16) The reaction of $FeCl_2$ with H(Mabiq) in mixtures of MeCN/CH_2Cl_2 or MeCN only leads to dark green solutions after several hours stirring. However, a mixture of products always results even when CH_2Cl_2 is avoided. A single crystal of Fe^{II}(Mabiq)(MeCN)Cl was isolated as a product of recrystallization of the green solid product from CH_2Cl_2/diethyl ether. Structural details can be found in the Supporting Information, Figure S2 and Table S1. Upon addition of CH_2Cl_2 to crude solids of Fe^{II}(Mabiq)(MeCN)Cl or **4a**, the solutions become red, with spectral features similar to **3**.

Scheme 2. .

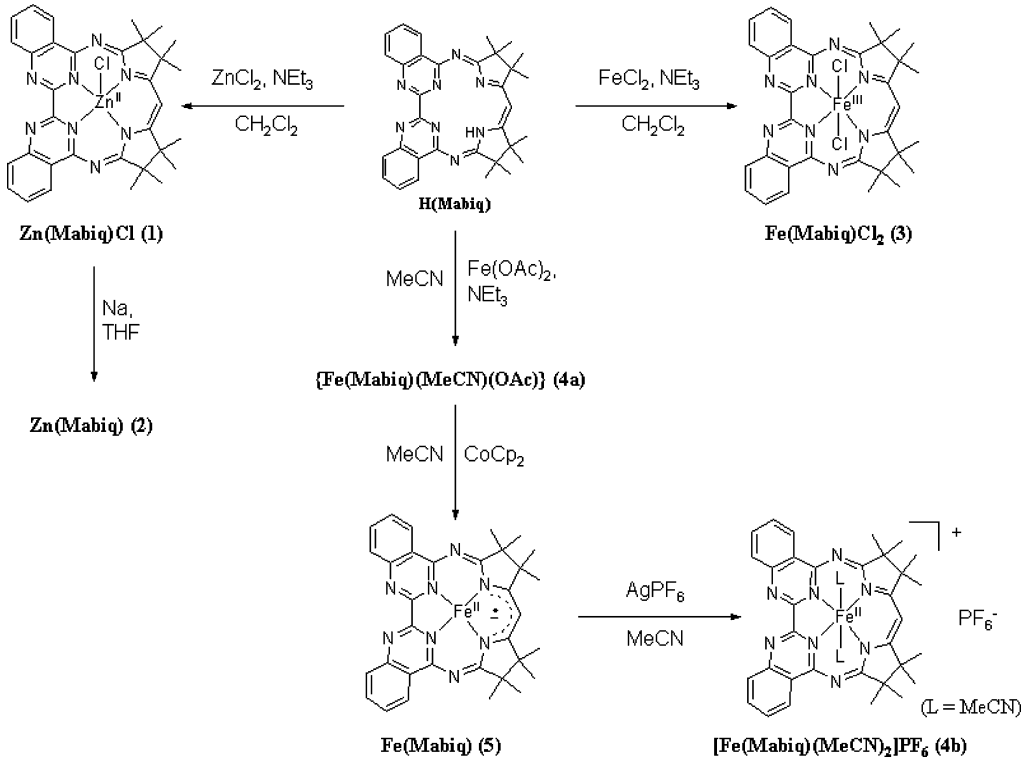

A cleaner route to the synthesis of the Fe^{II}-Mabiq compound ultimately was provided via the re-oxidation of the fully reduced Fe species, **5** (**5** = [Fe^{II}(Mabiq)], the synthesis of which stems from the one-electron reduction of **4a**, and is described below). Upon addition of a stoichiometric amount of $AgPF_6$ to a suspension of **5** in MeCN, the solution turns dark green as the product is solubilized by acetonitrile. The electronic spectrum of the product, [Fe(Mabiq)$(MeCN)_2$]PF_6 (**4b**), is identical to that of **4a** (Figure 2). The central unit of both **4a** and **4b** is an [Fe(Mabiq)]$^+$, and both compounds containing this moiety are generically designated as **4**. The two compounds differ only in the nature of the counteranion; the acetate may coordinate to the iron in **4a**, whereas **4b** contains two metal-bound acetonitrile groups and a non-coordinating PF_6 ion.

The addition of a stoichiometric amount of cobaltocene to crude solutions of the putative [Fe^{II}(Mabiq)(MeCN)(OAc)] (**4a**) in MeCN leads to the precipitation of a blue-green solid corresponding to the one-electron reduced [Fe^{II}(Mabiq)] (**5**). The electronic spectrum of turquoise solutions of **5** (Figure 2) in THF includes an absorption band at 624 nm, but lacks the more intense features between 400−500 nm observed in the spectra of **4**.

Solid State Structures. The crystal structure of the [Zn^{II}(Mabiq)Cl] complex (**1**) is shown in Figure 3 and the

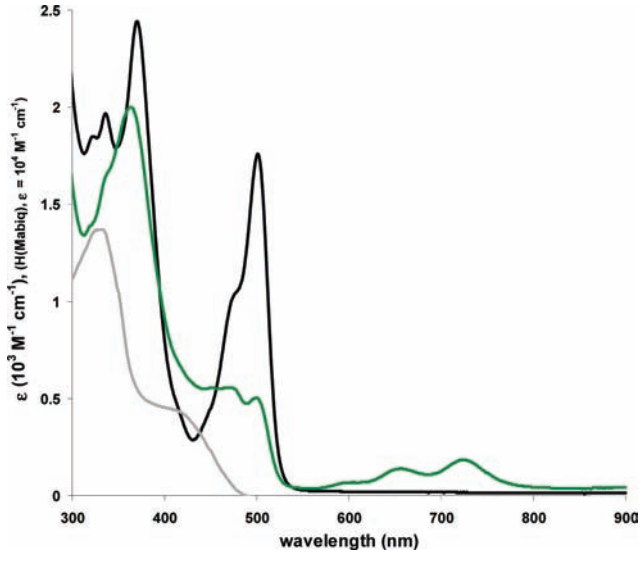

Figure 1. Electronic Spectra of H(Mabiq) (gray) in CH_2Cl_2, **1**, [Zn(Mabiq)Cl] (black) in CH_2Cl_2 and **2**, [Zn(Mabiq)] (green) in THF.

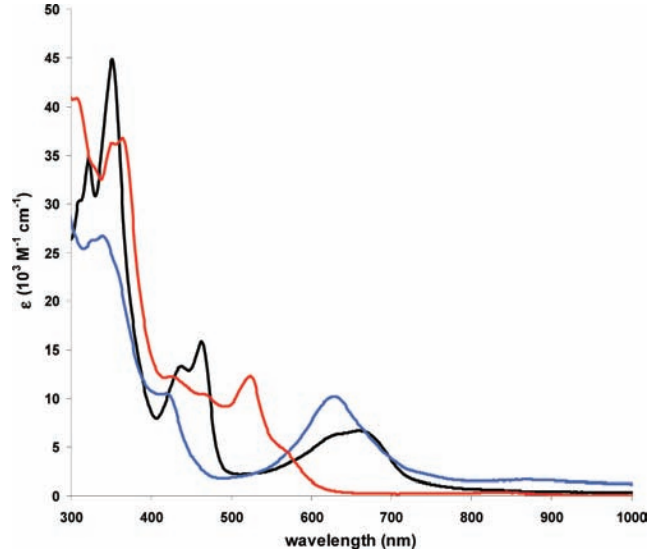

Figure 2. Electronic spectrum of Fe-Mabiq complexes: **3**, [Fe(Mabiq)Cl_2] (red) in CH_2Cl_2; **4b**, [Fe(Mabiq)$(MeCN)_2$]PF_6 (black) in MeCN; and **5**, [Fe(Mabiq)] (blue) in THF.

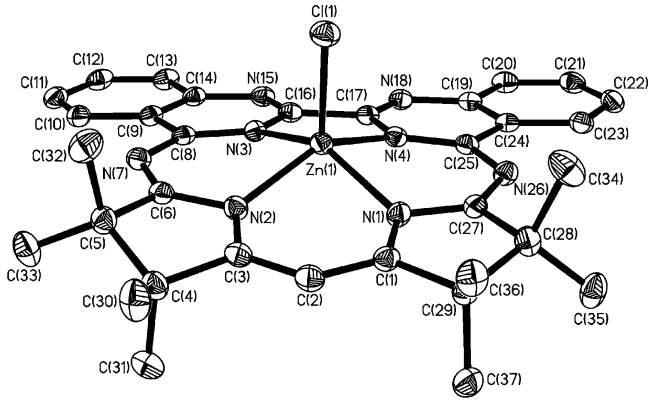

Figure 3. Crystal structure of **1**, [Zn(Mabiq)Cl].

crystallographic data is listed in Table 1. The coordination about the metal is square pyramidal; the Zn(II) ion sits 0.62 Å above the N_4-plane that comprises the macrocyclic cavity. The bipyrimidine unit is canted downward at an angle of ~11.5° from the coordinating nitrogens. A slight asymmetry is observed in the Zn−N bonds, with a longer bond of 2.09 Å to the bipyrimidine nitrogen atoms (N3, N4) versus a 2.03 Å bond to the diketiminate N-atoms (N1, N2). The asymmetry in metal−nitrogen bond lengths arises from differences in basicity for the two types of nitrogen donors, as observed for the [Co(Mabiq)$(CN)_2$] complex.[12] The bond lengths of the diketiminate unit lie between typical distances for the double- and single-bonded atoms, consistent with a fully conjugated structure: the C1−C2 and C2−C3 distances are at 1.40 Å and the average N1−C1 and N2−C3 distance is 1.354 Å. Solvent molecules are located in the structure of **1** in a ratio of 0.6 CH_2Cl_2 and 0.4 H_2O per Zn molecule.

The crystal structures and data for the Fe complexes are given in Figure 4 and Table 1. In all structures, the Fe lies within the plane of the macrocyclic N-donor atoms. Compounds **3** and **4b** are 6-coordinate pseudo-octahedral. Two crystallographically independent complex molecules of [Fe^{III}(Mabiq)Cl_2] (**3**) are observed in the unit cell that differ in the buckling of the byrimidine unit. In one conformer the two quinazoline units of the bipyrimidine essentially lie within the coordinating N_4 plane but are more distorted in the second conformer. A 3.61° difference in coplanarity results. Two non-coordinating solvent molecules (CH_2Cl_2) also are present in the crystal structure of **3**. The Mabiq ligand of **4b** also is distorted; the macrocycle is slightly buckled, with one pyrimidine group bent at a ~7° angle away from the plane of the second pyrimidine. The methyl groups in the dihydropyrrole backbone of **3** and **4b** are arranged in the syn conformation (depicted below).

The iron center in **5** is 4-coordinate square planar, having lost both axial ligands upon reduction. The bipyrimidine unit displays minimal distortion, and the methyl groups of the dihydropyrrole units are staggered (anti conformation).

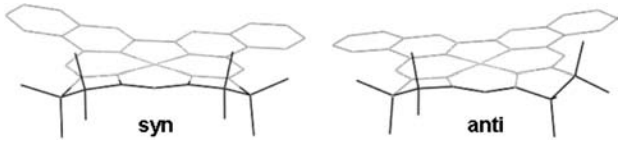

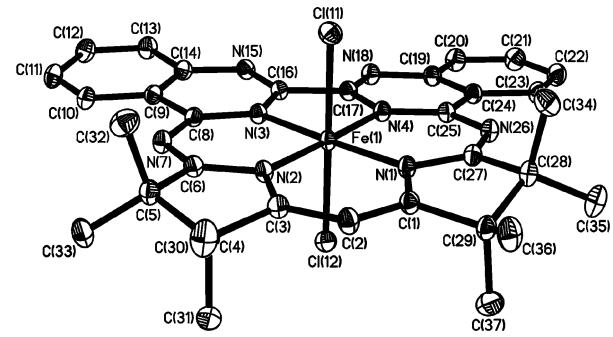

3) Fe(Mabiq)Cl_2

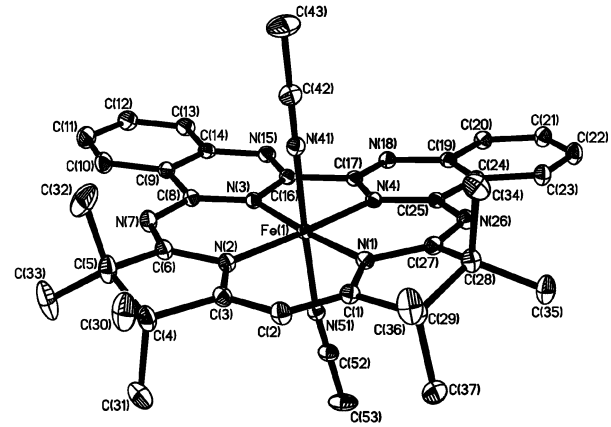

4b) [Fe(Mabiq)$(MeCN)_2$]$^+$

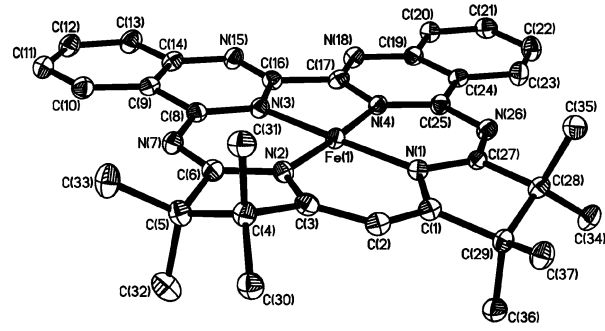

5) Fe(Mabiq)

Figure 4. Solid state structures of the Fe-Mabiq compounds. Top: [Fe^{III}(Mabiq)Cl_2] (**3**), middle: [Fe^{II}(Mabiq)$(MeCN)_2]^+$ (**4b**), bottom: [Fe(Mabiq)] (**5**).

The M−N distances show little variation among the series of Fe complexes. A slight decrease in bond lengths is observed with each reduction of the complexes, such that: [Fe^{III}(Mabiq)Cl_2]; Fe−N_{avg} = 1.93 > [Fe^{II}(Mabiq)-$(MeCN)_2]PF_6$; Fe−N_{avg} = 1.925 > [Fe^{II}(Mabiq)]; Fe−N_{avg} = 1.90. The bond distances within the Mabiq macrocycle also are comparable among the three Fe compounds. The most notable change in bond lengths is observed in the diketiminate-unit of **5**, where a slight shortening of the C−C bonds (C1−C2, C2−C3) and a lengthening of the C−N bonds (N1−C1, N2−C3) is apparent, compared to the analogous bond distances in **3** and **4b**.

Electrochemistry. Zn Complexes. The cyclic voltammogram (CV) of **1** exhibits a reversible one-electron redox wave centered at −1.4 V versus Fc^+/Fc (Figure 5, top; scan

Table 1. Crystallographic Data for **1**, **3**·CH_2Cl_2, **4b**·1.5CH_3CN, and **5**

	1·0.6CH_2Cl_2·0.4H_2O	**3**·CH_2Cl_2	**4b**·1.5CH_3CN	**5**
chem. formula	$C_{33.6}H_{35}Cl_{2.2}N_8O_{0.4}Zn$	$C_{34}H_{35}Cl_4FeN_8$	$C_{40}H_{43.5}F_6FeN_{11.5}P$	$C_{33}H_{33}FeN_8$
Fw	700.66	753.35	886.18	597.52
space group	$P2_1/c$, No. 14	$P1$, No. 2	$P2_1/n$, No. 14	$Pbca$, No. 61
a, Å	11.1513(4)	10.0858(3)	12.7450(9)	9.7687(6)
b, Å	21.3607(9)	18.6810(6)	16.2154(11)	20.6825(13)
c, Å	15.4174(6)	19.5964(7)	21.2095(14)	27.084(2)
α, deg	90	101.413(3)	90	90
β, deg	110.843(3)	104.352(3)	110.649(2)	90
γ, deg	90	102.852(3)	90	90
V, Å	3432.1(2)	3359.9(12)	4101.7(5)	5472.1(6)
Z	4	4	4	8
T, K	100(2)	100(2)	100(2)	100(2)
ρ calcd, g cm^{-3}	1.356	1.489	1.435	1.451
refl. collected/2_{max}	57527/60.00	93107/65.00	204018/65.00	107680/52.88
unique refl./$I > 2\sigma(I)$	9982/7352	24280/19103	14834/12931	5609/3654
no. of params/restr.	432/2	883/6	630/474	387/0
λ, Å /μ(Kα), cm^{-1}	0.71073/9.24	0.71073/8.06	0.71073/4.80	0.71073/5.92
R1 [a]/goodness of fit [b]	0.0513/ 1.025	0.0513/ 1.050	0.0541/ 1.149	0.0396/ 1.185
wR2 [c] ($I > 2\sigma(I)$)	0.1170	0.1312	0.1386	0.0850
residual density, e $Å^{-3}$	+0.74/−0.80	+1.10/−0.93	+1.18/−1.15	+0.43/−0.41

[a] Observation criterion: $I > 2\sigma(I)$. $R1 = \sum||F_o| - |F_c||/\sum|F_o|$. [b] $GoF = \{\sum[w(F_o^2 - F_c^2)^2]/(n - p)\}^{1/2}$. [c] $wR2 = \{\sum[w(F_o^2 - F_c^2)^2]/\sum w(F_o^2)^2\}^{1/2}$ where $w = 1/\sigma^2(F_o^2) + (aP)^2 + bP$, $P = (F_o^2 + 2F_c^2)/3$.

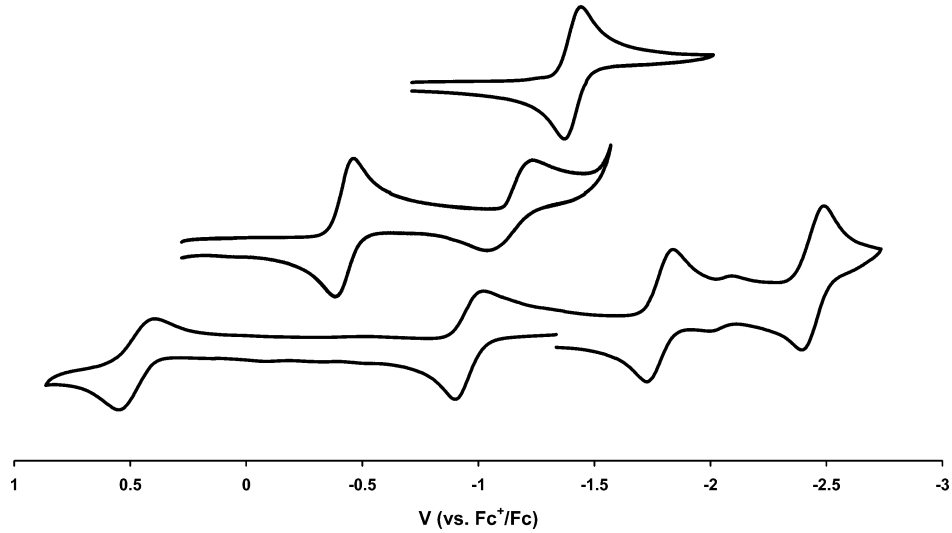

Figure 5. CV of **1** (top); 0.2 V/s, 0.1 M $TBAPF_6$, CH_2Cl_2, **3** (middle); 0.1 V/s, 0.1 M $TBAPF_6$ plus excess TBACl, CH_2Cl_2 and **5** (bottom); 0.1 V/s, 0.1 M $TBAPF_6$, THF. Glassy carbon working electrode.

rate = 0.1 V/s, 0.2 M $TBAPF_6$ (tetrabutylammonium hexafluorophosphate), CH_2Cl_2), as well as an additional irreversible reductive process beyond −2 V (E_p = −2.19 V, not shown). Both electron transfer processes are assigned as ligand-centered reductions. Electrochemical reduction (coulometry at −1.4 V vs $Ag/AgNO_3$) of [Zn(Mabiq)Cl] in CH_2Cl_2 coincides with a color change from orange to green. The one-electron reduced species contains features in the UV−vis spectrum (Supporting Information, Figure S4) that are identical to the product of chemical reduction of **1** using Na, to generate **2**. The EPR spectrum of the electrochemically generated species contains a distinct g = 2.006 signal, indicative of an organic radical. The EPR spectrum is reproduced by chemical reduction of **1** with Na (Supporting Information, Figure S5).

Fe Complexes. Three irreversible reductive peaks ($E_{1/2}$ = −0.46, −1.23, and −1.38 V; scan rate = 0.1 V/s; 0.2 M $TBAPF_6$, CH_2Cl_2) are observed in the CV of [Fe^{III}(Mabiq)Cl_2] (**3**), each corresponding to one-electron reductions. The first redox wave at −0.46 V becomes reversible in the presence of excess tetrabutylammonium chloride (Figure 5, middle, only first two redox waves shown), suggesting the loss of at least one chloride ligand upon reduction. The electrochemically generated product of controlled coulometry of **3** in CH_2Cl_2, at potentials corresponding to the first reduction, exhibits spectral features in the UV−vis region identical to **4** (Supporting Information, Figure S6).

The CV of **4b** in MeCN (Supporting Information, Figure S7) displays three reversible redox waves at 0.616, −1.3, and −1.638 V, as well as an irreversible wave at −1.94 V (scan rate = 0.1 V/s, 0.2 M $TBAPF_6$). The first wave is associated with a one-electron oxidation, while the negative potentials correspond to reductive processes. The CV of **4a** is nearly identical, the first two reductions occur at −1.37 and −1.62 V (scan rate = 0.1 V/s, 0.2 M $TBAPF_6$, MeCN), while oxidation occurs at 0.577 V. Coulometry of **4** at potentials corresponding to the first one-electron reduction

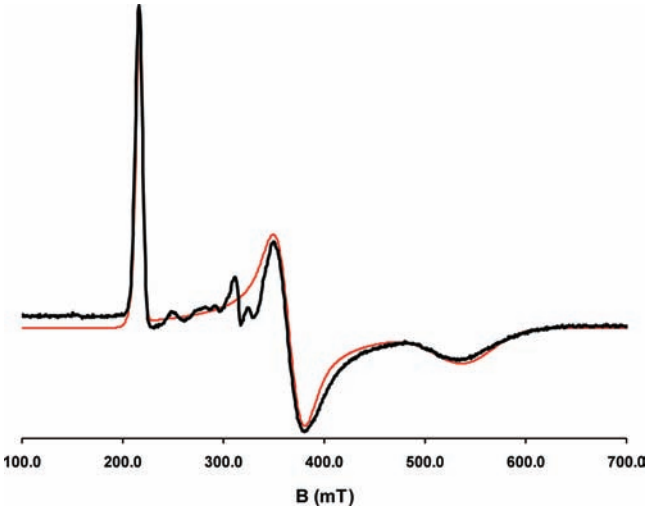

Figure 6. EPR spectrum of **3** in 1:1 THF:toluene; 10 K, frequency = 9.45 GHz, mod. amp. = 25 G, power = 0.05 mW. Black = experiment, red = simulation.

leads to the formation of **5**, as evident from the electronic spectrum (Supporting Information, Figure S8). The EPR spectrum of the electrochemically reduced product affords three g values with $g_{iso} = 2.09$. Although the second, presumably ligand-centered, reduction appears reversible, further coulometry led to decomposition of the Fe-Mabiq moiety.

Solutions of [Fe(Mabiq)] (**5**) in THF display four distinct electron transfer processes in the CV (Figure 5, bottom), centered at 0.454 V, −0.93 V (one-electron oxidations), −1.79 and −2.45 V (one-electron reduction processes, scan rate = 0.1 V/s, 0.2 M $TBAPF_6$). All four redox processes become reversible in the absence of axial ligands to the iron center. The first oxidation (coulometry at −0.2 V vs Ag/$AgNO_3$) generates a species whose absorption spectrum matches that of **4** (Supporting Information, Figure S9). Further oxidation or reduction of [Fe(Mabiq)] solutions proved prohibitive.

Magnetic Susceptibility and Electronic Structure Measurements. Spectroscopic data for the fully oxidized [Fe^{III}(Mabiq)Cl_2] (**3**) support the presence of a low-spin ferric center. The $S = 1/2$ ground state of **3** is confirmed by magnetic susceptibility measurements, which afford a temperature independent $\mu_{eff} = 1.93\ \mu_B$ (2−300 K, 1 T) and $g = 2.25$ from the data simulation (Supporting Information, Figure S10). A large rhombic anisotropy of the g-tensor is apparent from the EPR spectrum of **3** (Figure 6) with three distinct g values observed at 3.09, 1.84, and 1.25. The high $g_{max} > 3$ and the broad absorption lines at lower field are characteristic of HALS (highly anisotropic low spin) species that are associated primarily with ferric heme complexes.[17,18]

The Mössbauer spectrum of **3** exhibits an isomer shift of $\delta = 0.20$ mm/s and a quadrupole splitting, $\Delta E_Q = 2.86$ mm/s, at 80 K. The spectrum is asymmetric at low temperatures. The equivalent intensity of the two peaks at higher temperature (373 K; $\delta = 0.10$ mm/s, $\Delta E_Q = 2.72$ mm/s,

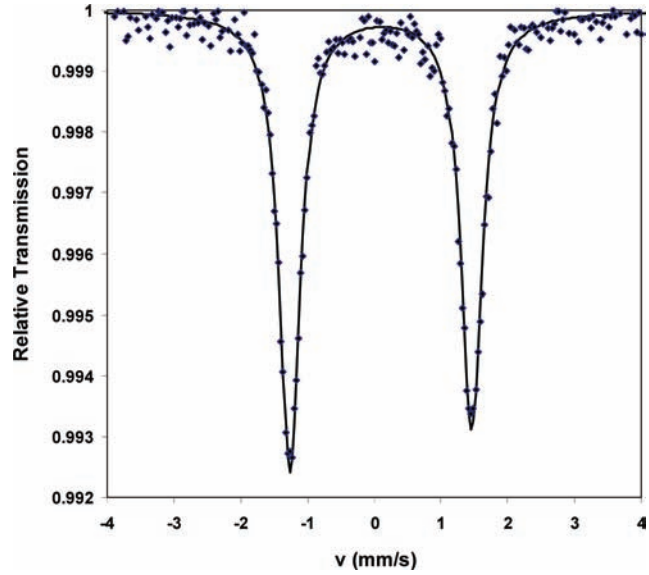

Figure 7. Mössbauer spectrum of **3**; 373 K, $\delta = 0.10$ mm/s, $\Delta E_Q = 2.72$ mm/s.

Figure 7) reveals intermediate to fast spin relaxation. The isomer shift for **3** correlates well with reported values for low-spin ferric heme sites.[19] The experimentally derived Mössbauer values also are closely matched by DFT calculations on the low-spin [Fe^{III}(Mabiq)Cl_2] complex (calculated $\delta = 0.27$ mm/s, $\Delta E_Q = 2.82$ mm/s).

With one electron more than its ferric-dichloro counterpart (**3**), compound **4** can be considered as either an Fe^{II}(Mabiq) complex or as Fe^{III}(Mabiq$^{\bullet}$), a trivalent iron center coordinated to the Mabiq radical-dianion. The former depiction signifies a metal-centered reduction, whereas the macrocyclic ligand acquires the additional electron in the latter scenario. Magnetic susceptibility data for **4b** ([Fe(Mabiq)$(MeCN)_2$]PF_6) establishes a diamagnetic ground state for this complex and signifies a low-spin iron center for either of the two electronic structures in question. The zero-field Mössbauer spectrum of **4b** exhibits an isomer shift of 0.34 mm/s and a quadrupole splitting, $\Delta E_Q =$ 1.8 mm/s (Figure 8).[20] The isomer shift observed in the Mössbauer spectra of **4** falls within the range of values commonly observed for both low-spin ferric or low-spin ferrous N_4-coordinating complexes.[19,21] Thus, neither electronic structure description can be excluded on the basis of the Mössbauer data for this diamagnetic compound.

Compound **5** is the product of the subsequent reduction process and two alternate electronic structures are at issue again: an Fe^{I}(Mabiq) complex or an Fe^{II}(Mabiq$^{\bullet}$) species, the iron center in the latter representation is coordinated by the ligand radical-dianion. Magnetic susceptibility data for **5** (Supporting Information, Figure S12) yield a value of μ_{eff}

(17) Safo, M. K.; Gupta, G. P.; Walker, F. A.; Scheidt, W. R. *J. Am. Chem. Soc.* **1991**, *113*, 5497.
(18) Walker, F. A.; Huynh, B. H.; Scheidt, W. R.; Osvath, S. R. *J. Am. Chem. Soc.* **1986**, *108*, 5288.
(19) Debrunner, P. G. In *Iron Pophyrins*; Lever, A. B. P., Gray, H. B., Eds.; John Wiley & Sons: 1989; Vol. Part *3*.
(20) Mössbauer data also was collected for the putative [Fe(Mabiq)(MeCN)(OAc)] species (**4a**), which yields an isomer shift of 0.36 mm/s and $\Delta E_Q = 1.97$ mm/s (Supporting Information, Figure S11). The nature of the counteranion does not alter the electronic structure of compound **4**, as corroborated by the identical UV-vis absorption spectra of the two complexes.
(21) Dabrowiak, J. C.; Merrell, P. H.; Stone, J. A.; Busch, D. H. *J. Am. Chem. Soc.* **1973**, *95*, 6613.

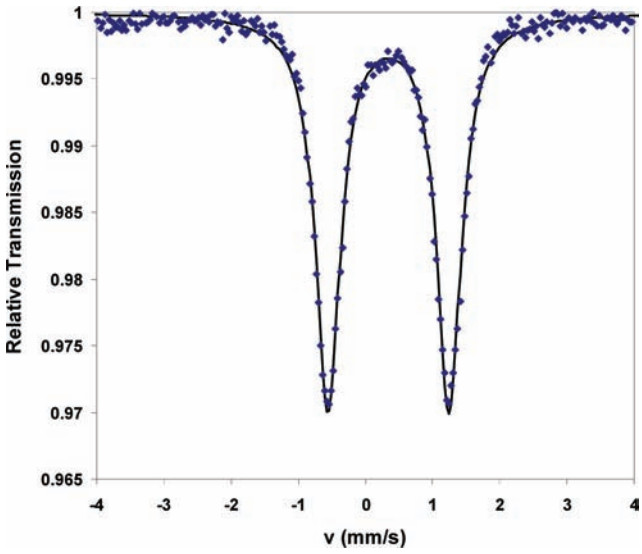

Figure 8. Mössbauer Spectrum of **4b**; 80 K, $\delta = 0.34$ mm/s, $\Delta E_Q = 1.8$ mm/s.

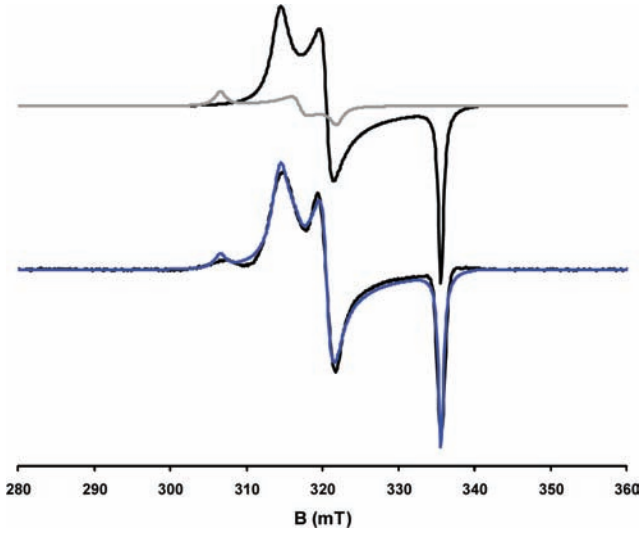

Figure 9. EPR spectrum of **5** in 1:3, THF:toluene; 30 K, frequency = 9.43 GHz, mod. amp. = 10 G, power = 0.4 mW. Top: simulated spectra of the two individual subcomponents. Bottom: experimentally obtained spectrum (black) and combined simulated data (blue).

$= 2.0\ \mu_B$ (1 T, 2−300K) and can be simulated reasonably well with $S = 1/2$ and $g = 2.29$.[22] The overall $S = 1/2$ spin state allows for either low-spin (Fe^I or Fe^{II}) or intermediate spin (Fe^{II}) at the iron center. The unpaired electron occupies a metal-based orbital for an Fe^I complex, whereas for a low-spin Fe^{II} species the singly occupied molecular orbital (SOMO) is ligand-centered. Antiferromagnetic coupling between the ferrous center and the ligand π-radical anion accounts for the total spin of $S_T = 1/2$ in the case of an intermediate spin Fe^{II} formulation. The EPR spectrum of **5** (Figure 9) denotes significant effects of spin−orbit coupling in the ground state of the square planar complex and affords

(22) The sharp rise seen in the μ_{eff} vs T plot from 0−6 K (Supporting Information, Figure S12) can be attributed to solid-state intermolecular interactions and requires the theta Weiss value to properly fit the data. The crystal packing structure of compound **5** reveals pairs of Fe molecules separated by a distance of 3.325 Å as evidence for dimeric interactions.

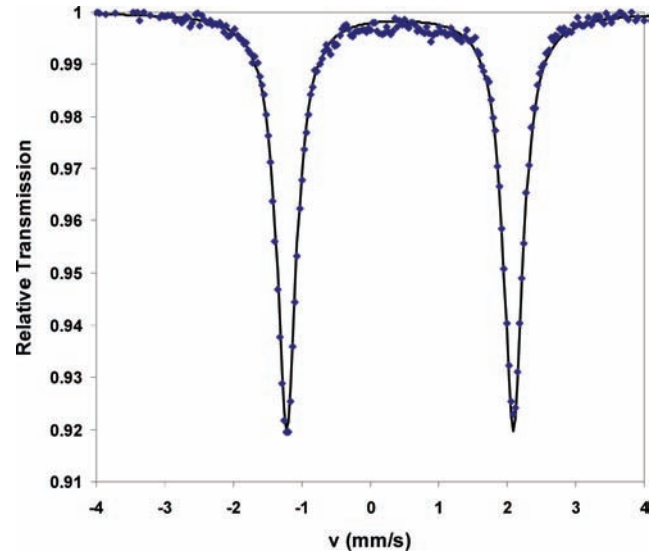

Figure 10. Mössbauer Spectrum of **5**; 80 K, $\delta = 0.43$ mm/s, $\Delta E_Q = 3.31$ mm/s.

g values of 2.14, 2.10, and 2.01.[23] The data clearly demonstrates a large contribution from the metal center to the paramagnetism of this complex, in contrast to the reduced Zn(Mabiq$^{\bullet}$) complex where the unpaired electron is localized purely on the ligand. This factor rules out the possibility of an $S = 0$ spin state at the iron. The μ_{eff} value resulting from the magnetic susceptibility data is slightly higher than the spin-only value of 1.73 μ_B for an $S = 1/2$ system, consistent with the presence of antiferromagnetic interactions in this complex. An alternate fit to the data takes into account the description of **5** as containing an intermediate spin Fe^{II} center antiferromagnetically coupled to a ligand-based radical, with $S_{Fe} = 1$, $S_L = 1/2$, and $S_{tot} = 1/2$. The data simulation with these parameters affords an estimate of the coupling constant, $-J > 500\ cm^{-1}$, a value for $g_{Fe} = 2.21$ and $g_L = 2.0$; the J value illustrates strong coupling between the iron center and the Mabiq radical.

The Mössbauer spectrum for **5** (Figure 10) exhibits an isomer shift of 0.43 mm/s, and $\Delta E_Q = 3.31$ mm/s. The isomer shift value is typical of a divalent Fe center and both Mössbauer parameters are similar to values previously reported for intermediate spin Fe^{II} complexes (for example: Fe^{II}(porphyrinogen),[15] $\delta = 0.35$, $\Delta E_Q = 2.34$ mm/s; Fe^{II}(phthalocyanine),[19] $\delta = 0.39$, $\Delta E_Q = 2.62$ mm/s). The isomer shift is reproduced by DFT calculations for complex **5** ($\delta_{calc} = 0.44$ mm/s) using the broken symmetry (BS(2,1)) formalism. The experimentally determined quadrupole splitting is significantly larger than the value calculated by DFT (calculated $\Delta E_Q = 1.81$ mm/s) but comparable to the value reported for ferrous-phthalocyanine.[19]

Discussion

Zn-Mabiq Compounds. The divalent Zn-Mabiq compounds provide an ideal reference to investigate the properties

(23) The EPR spectrum indicates the presence of two components, in a ratio of 9:1, likely due to the presence of conformers of **5** in solution. The fit for each component is shown in Figure 9 (top). The minor species afford g values = 2.2, 2.13 and 2.09.

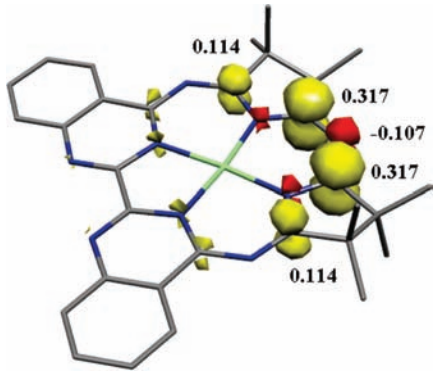

Figure 11. DFT-derived (UKS calculation) spin density map for **2**, [Zn(Mabiq)] based on Loewdin spin population analysis.

of the macrocyclic biquinazoline ligand. The redox inertness of zinc denotes less electronic structure complexity than for the corresponding Fe-Mabiq compounds. The zinc complexes thus were intended as a probe for the spectroscopic and redox features associated with the Mabiq ligand.

It is surprising, then, that coordination of Zn^{II} to the macrocycle leads to a dramatic change in the electronic spectrum compared with that of the free ligand. Neither solutions of the protonated H(Mabiq) nor solutions of the deprotonated Mabiq ligand absorb at wavelengths past 500 nm (Supporting Information, Figure S3), whereas the [Zn^{II}(Mabiq)Cl] complex strongly absorbs at 502 nm. The effect of Zn coordination to the Mabiq molecule contrasts with the effect of Zn complexation to the porphyrins and phthalocyanines, where only a slight red-shift of the ligand π-π* transitions is observed.[9,24] Metal-to-ligand charge-transfer (MLCT) or ligand-to-metal charge transfer (LMCT) transitions can be ruled out as an explanation for the new absorption features of the zinc complex. The electronic spectrum of **1** closely resembles that of the [Co^{III}(Mabiq)-$(CN)_2$] complex,[12] which also features absorption bands at 502 and 536 nm. These transitions were ascribed to the effect of the net charge of the Co^{III} ion on the energy of the ligand π-π* transitions. However, this explanation seems inadequate to describe the disparate intensity and band-shape of the new absorption features compared with those of the free ligand. As compound **1** also is highly fluorescent, further photophysical and theoretical studies are currently underway, which may provide insight into the nature of the electronic transitions of this complex.

The [Zn^{II}(Mabiq)Cl] compound can be one-electron reduced both chemically and electrochemically to generate compound **2**, described as [Zn^{II}(Mabiq$^{\bullet}$)]. The EPR spectrum of **2** unequivocally establishes the presence of an unpaired ligand-centered electron, providing the first attest to the redox non-innocence of the macrocyclic biquinazoline molecule. DFT-derived spin density maps illustrate that the unpaired electron of compound **2** is localized purely on the diketiminate half of the macrocycle (Figure 11). Comparison of the frontier orbitals of **1** and **2** (Figure 12) shows that the unpaired electron in **2** occupies a former ligand based lowest unoccupied molecular orbital (LUMO) of **1**: this orbital consists primarily of p-orbitals of the diketiminate unit. The electronic spectrum of **2** presents new absorption bands at 600−800 nm. Metal-diimine radical complexes absorb strongly in this region; the low-energy features are assigned as intraligand π-π* charge transfer transitions, typical of this class of complexes.[13] A bipyrimidine-centered π*-orbital constitutes the LUMO of the reduced zinc complex (Figure 12B). It is plausible that the low energy transitions in the spectrum of **2** stem from an intramolecular charge transfer transition between these two orbitals. In fact, the nature of the frontier orbitals is consistent for **2** and **5**, the fully reduced iron complex also found to have ligand radical character and which exhibits absorption bands in this region (vide infra). However, a precise assignment of these transitions requires time-dependent density-functional theory (TD-DFT) methods.

Fe-Mabiq Compounds. Spectroscopic and structural data for the [Fe^{III}(Mabiq)Cl_2] compound depict a highly anisotropic low-spin ferric center, akin to the ferric-porphyrin systems. Electron density maps obtained from DFT calculations confirm the presence of the unpaired electron in a purely metal-centered orbital. The DFT derived molecular orbital (MO) diagram (Figure 13) illustrates that the asymmetry of the ligand leads to non-degenerate d_{xz}, d_{yz} orbitals: in contrast to the essentially non-bonding d_{yz} orbital, d_{xz} shows significant anti-bonding interactions with the diketiminate nitrogen p-orbitals. The characteristic HALS spectra arise from the near degeneracy of the d_{xz}/d_{yz} orbitals, imposed by the axial ligands of the low-spin ferric heme complexes.[18] In the ferric-Mabiq complex, we estimate the tetragonal splitting parameters Δ, and the rhombic splitting parameter V, as 5.53 λ and 1.42 λ respectively, on the basis of EPR g values for **3**.

One-electron removed from the ferric-Mabiq complex is compound **4**, which can be generated upon reduction of **3** or via oxidation of **5**. Two forms of this species have been investigated, of the general form [Fe(Mabiq)$(MeCN)_n$](X), where X = OAc or PF_6, n = 1−2. At the core of these compounds is the [Fe(Mabiq)]$^+$ moiety. The simplest formulation of this diamagnetic complex consists of a low-spin Fe^{II} center. However, the demonstrated redox non-innocence of the Mabiq ligand, on the basis of the [Zn^{II}(Mabiq$^{\bullet}$)] complex, raised the possibilty of an alternate description of **4** as containing an [Fe^{III}(Mabiq$^{\bullet}$)]$^+$ moiety and entails the reduction of the ligand.

The low-energy absorption bands (600−700 nm) in the electronic spectrum of **4** are reminiscent of the intraligand charge transfer transitions in metal diimine-radical complexes. The fact that the [Zn(Mabiq$^{\bullet}$)] complex and the fully reduced Fe-Mabiq compound (**5**) both share these low-energy features with the spectrum of **4** lent credence to the argument for an [Fe^{III}(Mabiq$^{\bullet}$)]$^+$. The Mössbauer parameters for compound **4** are consistent with either possible electronic structure. However, a broken symmetry solution in support of the [Fe^{III}(Mabiq$^{\bullet}$)]$^+$ formulation was not obtained from DFT calculations on [Fe(Mabiq)$(MeCN)_2$]$^+$. The DFT-derived MO scheme (Figure 14) shows three doubly occupied orbitals of the t_{2g} set (O_h symmetry), in favor of a low-spin

(24) Lever, A. B. P. In *Advances in Inorganic and Radiochemistry*; Emeleus, H. J., Sharpe, A. G., Eds.; Academic Press: New York, 1965; Vol. 7, pp 28−105.

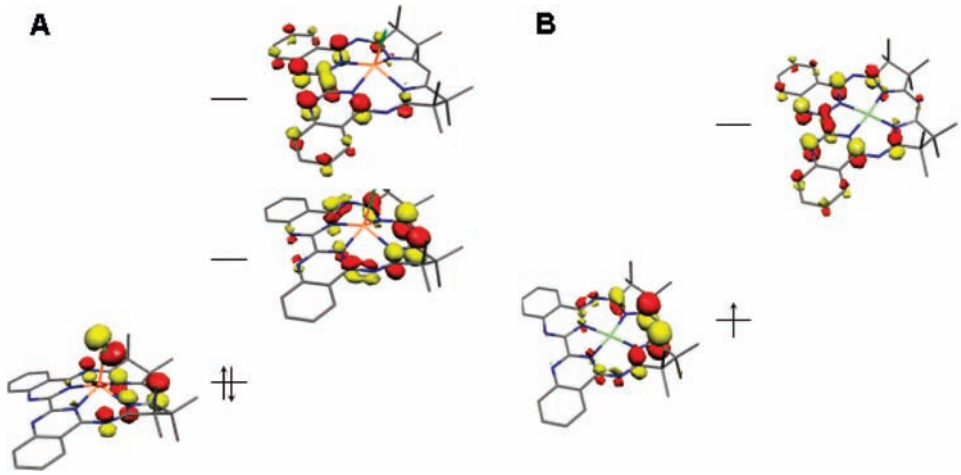

Figure 12. DFT-derived (UKS) MO scheme depicting the frontier orbitals of **1**, [Zn(Mabiq)Cl] (A) and **2**, the reduced [Zn(Mabiq)] (B).

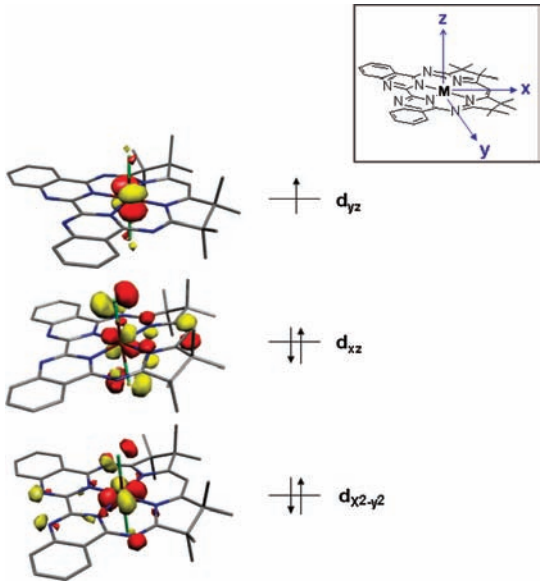

Figure 13. Qualitative MO diagram derived from UKS calculation of **3**, [Fe(Mabiq)Cl_2].

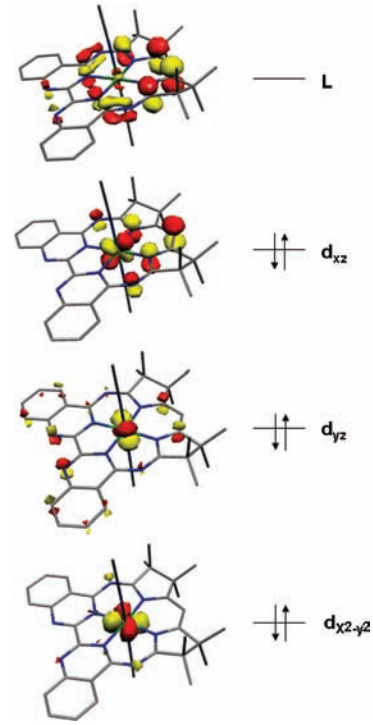

Figure 14. Qualitative MO diagram derived from DFT calculation (UKS) of $[Fe(Mabiq)(MeCN)_2]^+$.

Fe^{II} center. The crystal structure also supports a low-spin Fe^{II} species since the bond distances of the ligand-diketiminate unit are nearly identical to those of the $[Fe^{III}(Mabiq)Cl_2]$ complex. The similarity of the low energy transitions in the absorption spectrum to those observed in the electronic spectra of compounds **2** and **5** appear to be purely coincidental.

Compound **5** also can be described by either of two redox formulations, a low-valent $[Fe^{I}(Mabiq)]$ or by $[Fe^{II}(Mabiq^{\bullet})]$; the latter formulation again indicative of a ligand-centered reduction. The analogous distinction between an Fe^{I} and an Fe^{II}-π-radical anion has been a long-standing dilemma in the assignment of reduced iron-porphyrin systems, where conflicting data has complicated the assignment of their metal oxidation and spin states.[5,25,26] Fe^{I} species have been implicated in the chemistry of the hydrogenases;[27] however, only a few well-characterized examples of synthetic inorganic low-valent iron complexes are known.[28−30] The compound most relevant to the present studies is the Fe(I)-tetraphenylporphyrin complex, $[Fe^{I}(TPP)]^-$.[5] The metal coordination environment of $[Fe^{I}(TPP)]^-$ is similar to the fully reduced Fe(Mabiq) complex: a 4-coordinate square planar iron center ligated by a conjugated N_4-macrocycle and with an $S = 1/2$ ground state. The majority of the data for this compound support the presence of an Fe^{I}.

On the basis of spectroscopic data, the Fe^{I} formulation for **5** can be confidently discarded. A definitive deviation is observed for the Mössbauer data: the isomer shift of 0.41 mm/s obtained for **5** is substantially smaller than the value

(25) Reed, C. A. *Adv. Chem. Ser.* **1982**, 333.
(26) Srivatsa, G. S.; Sawyer, D. T.; Boldt, N. J.; Bocian, D. F. *Inorg. Chem.* **1985**, *24*, 2123.
(27) Rees, D. C. *Annu. Rev. Biochem.* **2002**, *71*, 221.
(28) Sadique, A. R.; Brennessel, W. W.; Holland, P. L. *Inorg. Chem.* **2008**, *47*, 784.
(29) Mankad, N. P.; Whited, M. T.; Peters, J. C. *Angew. Chem., Int. Ed.* **2007**, *46*, 5768.
(30) Kisko, J. L.; Hascall, T.; Parkin, G. *J. Am. Chem. Soc.* **1998**, *120*, 10561.

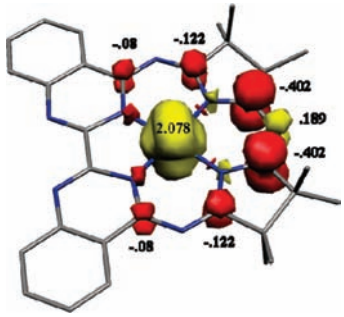

Figure 15. DFT-derived spin-density plot for **5** (BS(2,1) calculation) based on Loewdin spin population analysis.

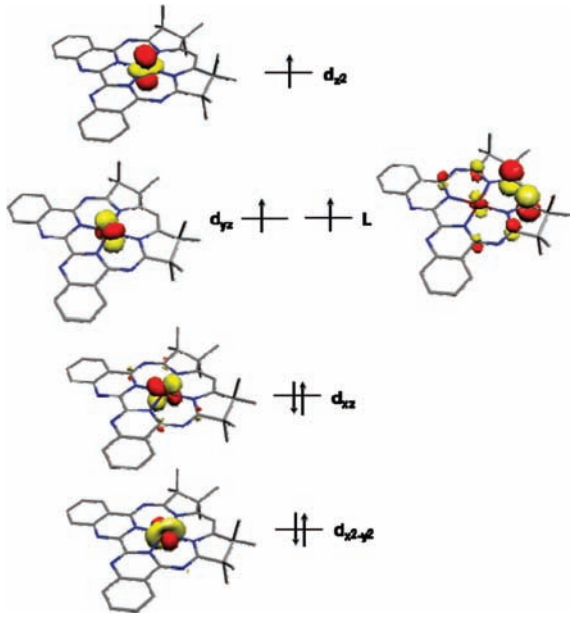

Figure 16. Qualitative MO diagram derived from BS(2,1) calculation of **5**, [Fe^{II}(Mabiq)].

of 0.6 mm/s for $[Fe^{I}(TPP)]^{-}$.[5] Most importantly, the Mössbauer values for the [Fe(Mabiq)] complex are comparable to the reported values for intermediate-spin Fe^{II} compounds containing macrocyclic-N_4 ligands.[15,19] The absorption band at 624 nm in the electronic spectrum of **5** again supports the presence of a ligand radical. A purely ligand-centered radical, however, would not give rise to the observed EPR spectrum and therefore must be strongly antiferromagnetically coupled to the $S = 1$ metal center.

The final testimony to the [Fe^{II}(Mabiq$^{\bullet}$)] formulation is provided by DFT calculations. The DFT-derived spin density map clearly depicts two unpaired spins on the Fe center, and one unpaired spin of opposite sign on the ligand (Figure 15). The ligand radical again is localized on the diketiminate unit, as seen in the spin density plot of the reduced Zn complex (**2**). The bond distances in the crystal structure of **5** follow the trend expected for the one-electron reduction of the Mabiq molecule at the diketiminate unit. In comparison to the bond distances of structures **3** and **4b**, the C−C bonds of the diketiminate unit are slightly longer, while the C−N bond lengths decrease.

The qualitative MO diagram (Figure 16) shows two singly occupied metal-based orbitals (d_{z^2} and d_{yz}) that account for the intermediate spin state at the iron. A corresponding ligand-centered SOMO of beta-spin has a spatial overlap of 0.4, with the Fe d_{yz} orbital. The enforced antiferromagnetic coupling between the Fe and the Mabiq radical gives rise to the $S = 1/2$ ground state of **5**.

Conclusions

Several features distinguish the asymmetric Mabiq ligand from the related porphyrin-type systems. The nitrogen groups of the Mabiq macrocycle are stronger donor ligands in comparison to the pyrrole units of the porphyrins and corroles, as evidenced by the low-spin configuration of the ferric-dichloro-Mabiq complex (**3**). In addition to the familiar $Fe^{III/II}$ redox chemistry of iron-containing N_4-tetradentate macrocyclic complexes, a third oxidation state is available to the iron-Mabiq series that clearly involves the redox participation of the ligand. In contrast to the porphyrins, where oxidation of the pyrrole-based macrocycles more commonly is observed, the Mabiq ligand readily acquires one electron. Reduction of the macrocyclic ligand was unambiguously demonstrated by the reduced [Zn^{II}(Mabiq$^{\bullet}$)] complex. In the corresponding [Fe^{II}(Mabiq$^{\bullet}$)] compound, the ligand radical-dianion stabilizes the rare intermediate-spin state of the divalent iron.

The unpaired electron of the Mabiq radical-dianion appears to be localized at the diketiminate portion of the macrocycle. Interestingly, low-coordinate Fe-diketiminate complexes containing oxo, imido, and hydride ligands have been isolated recently that display a promising potential as oxidation/reduction catalysts.[31] The redox participation of the diketiminate backbone in the chemistry of these complexes has never been observed. The additional conjugation of the Mabiq macrocycle is certain to play a significant role in the redox properties of this unique ligand. However, our studies demonstrate that the redox non-innocence of the diketiminates is a matter for consideration in the chemistry of metal complexes containing such ligands. The multiple redox and spin states available to the Fe-Mabiq complexes suggest a rich chemistry for these complexes.

Experimental Section

All reagents were purchased from Aldrich unless otherwise noted. All metal-containing compounds were prepared using standard glovebox techniques and dry solvents, except as noted.

H(Mabiq). 2-4:6-8-Bis(3,3,4,4-tetramethyldihydropyrrolo)-10-15-(2,2′-biquinazolino)-[15]-1,3,5,8,10,14-hexaene-1,3,7,9,11,14-N_6 (H(Mabiq)) was synthesized as previously described,[12] with the following modification: The dione precursor, 4,4′-dihydroxy-2,2′-biquinazoline, was synthesized from the oxalylbis(anthranilamide) by heating to ∼350 °C using a metal bath. Upon heating, water was released as steam, and the solid turned a dark gray-brown. Recrystallization of the resultant product resulted in a light brown solid (72% yield), which was confirmed to be the dione product by comparison to the previously reported IR data for this product. This material was used in the subsequent reaction to synthesize 4,4′-dichloro-2,2′-biquinazoline, without further purification and without any effect on the yield of the dichloro- product. Purity of all other compounds was verified by IR, mass spectrometry, and ^{1}H NMR spectroscopy and by comparison to the reported values.

(31) Holland, P. L. *Acc. Chem. Res.* **2008**, *41*, 905.

[Zn(Mabiq)Cl] (1). Triethylamine (13 μL) was added to a solution of H(Mabiq) (50 mg, 0.092 mmol) in dichloromethane (20 mL) under an argon blanketing atmosphere with constant stirring. After 10 min, $ZnCl_2$ (0.0126 g, 0.092 mmol) was added to the solution. The faint yellow solution was stirred for 3 h, during which time the solution gradually turned orange. The solvent was removed, and the product was recrystallized from dichloromethane-hexane (0.058 g, 90%). Single crystals were obtained from slow diffusion of hexane into dichloromethane solutions of **1**. ^{1}H NMR (400 MHz, $CDCl_3$): δ = 9.03 (d, 2H), 8.43 (d, 2H), 8.03 (dt, 2H), 7.78 (dt, 2H), 5.81 (s,1H), 1.55 (s, 6H), 1.42 (m,12H), 1.26 (s, 6H). ES-MS (*m*/*z*): 641 [M+H], 605 [M-Cl]; EI-MS (*m*/*z*): 640, 605. UV−vis λ_{max} (nm (ε, mM^{-1} cm^{-1})) in CH_2Cl_2: 337 (19.4), 370 (23.7), 471 (9.8), 502 (17.6) Anal. Calcd for [Zn(Mabiq)Cl]$\cdot$ 0.6(CH_2Cl_2)$\cdot$0.4(H_2O) = $C_{33.6}H_{35}N_8Cl_{2.2}O_{0.4}Zn$: C, 57.54; H, 4.99; N, 15.98. Found: C, 57.30; H, 5.05; N, 15.80. Elemental analysis run in duplicate with identical results.

[Zn(Mabiq)] (2). To a suspension of Zn(Mabiq)Cl (64 mg, 0.1 mmol) in THF was added Na (11.5 mg, 0.1 mmol, as 20% Na/Hg beads). After 36 h stirring the reaction mixture turned green as the product went into solution. The solution was filtered over celite, and the solvent was removed in vacuo, yielding a green solid, which was washed with a minimum amount of cold ether. (0.042, 68%) A purer solid could also be obtained upon precipitation of the product from THF with diethylether and subsequent filtration. EI-MS (*m*/*z*): 605, 575, 545. UV−vis λ_{max} (nm (ε, mM^{-1} cm^{-1})) in THF: 365 ($\sim$20), 477 (5.6), 501 (4.8), 600 (0.8), 655 (1.5), 727 (2.0) Anal. Calcd for [Zn(Mabiq)]$\cdot$ (THF) = $C_{37}H_{41}N_8OZn$: C, 65.44; H, 6.04; N, 16.50. Found: C, 65.47; H, 6.01; N, 16.45. Elemental analysis run in duplicate with identical results.

[Fe^{III}(Mabiq)Cl$_2$] (3). $FeCl_2$ (15 mg, 0.11 mmol) was added to a glass vessel containing H(Mabiq) (50 mg, 0.092 mmol) and 13 μL of NEt_3 in 20 mL of dichloromethane. The reaction was stirred for 1−2 days during which time the solution turned dark red. Crystalline material, used for all subsequent analysis, was obtained from slow diffusion of ether into the dichloromethane solution. Yield: 0.011 g (18%). ES-MS (*m*/*z*): 632 [M − Cl]. UV−vis λ_{max} (nm (ε (mM^{-1} cm^{-1})) in CH_2Cl_2: 310 ($\sim$41), 352 (31), 365 (31), 428 (8.6), 470 (7.3), 524 (8.6), 568 (sh), 836 (0.2). Anal. Calcd for [Fe(Mabiq)Cl$_2$]$\cdot$(CH_2Cl_2) = $C_{34}H_{35}Cl_4FeN_8$: C, 54.21; H, 4.68; N, 14.87. Found: C, 53.83; H, 5.19; N, 14.48.

[Fe^{II}(Mabiq)(OAc)(MeCN)] (4a). $Fe(OAc)_2$ (33 mg, 0.19 mmol) was added to a glass vessel containing H(Mabiq) (100 mg, 0.184 mmol) and 26 μL of NEt_3 in 15 mL of acetonitirile. After approximately 1 h of stirring the reaction mixture turned green. The reaction was allowed to proceed for at least 12 h, after which the solution was filtered over celite and the solvent removed in vacuo, yielding a green solid. The crude product, as isolated, is $\geq$78% pure, as indicated by both the Mössbauer (Supporting Information, Figure S11) and NMR spectrum (Figure S14). The crude product could not be recrystallized: it is highly soluble in acetonitrile, and the presence of other solvents results in a color change of the solutions, corresponding with possible decomposition of the product or ligand exchange (i.e, with THF). Therefore, product of suitable purity for elemental analysis could not be obtained. ^{1}H NMR (400 MHz, CD_3CN): aromatic δ = 9.24 (m, 2H), 8.35 (m), 8.12 (m), 7.96 (m), 7.87(m), 7.01 (s), 7.02 (s), aliphatic: δ = 1.5 (s), 1.53 (s). ES-MS (*m*/*z*): 656 [M − MeCN + H]$^+$, 597 [656 − OAc]$^+$. UV−vis, λ_{max} (nm) in CH_3CN: 352, 440, 465, 620, 660.

[Fe^{II}(Mabiq)(MeCN)$_2$]PF$_6$ (4b). A 1.1 equivalent of $AgPF_6$ (10 mg, 0.04 mmol) was added to a suspension of **5** (22 mg, 0.037 mmol) in 5 mL of acetonitrile. After approximately 3 h stirring the reaction mixture turned green as the product went into solution. The solution was filtered over celite, to remove the precipitated Ag, and the solvent removed in vacuo, yielding a green solid. Yield: 60%. Single crystals could be obtained by slow diffusion of ether into a solution of **4b** in acetonitrile. ^{1}H NMR (400 MHz, CD_3CN (1.96 ppm)): δ = 9.26 (d, 2H), 8.37 (d, 2H), 8.13 (t, 2H), 7.97 (t, 2H), 7.03 (s, 1H), 1.55 (s, 24H). UV−vis, λ_{max} (nm, (ε (mM^{-1} cm^{-1})) in CH_3CN: 310 (30), 322 (34), 351 (43), 437 (13.3), 464 (15.7), 630 (6.2), 665 (6.5). Anal. Calcd for $C_{37}H_{39}N_{10}FePF_6$: C, 53.89; H, 4.92; N, 16.89. Found: C, 53.80; H, 4.92; N, 16.89.

[Fe(Mabiq)] (5). To a solution of **4a** (0.056 mg, 80 mmol) in acetonitrile was added 1.1 equiv of $CoCp_2$ (16 mg, 85 mmol). After stirring overnight, a dark blue-green precipitate was observed, which was filtered away from the solution, washed with a minimal amount of cold MeCN, followed by hexane. Yield: 68%. The solid was recrystallized from vapor diffusion of hexane into THF. UV−vis λ_{max} (nm, (ε (mM^{-1} cm^{-1})) in THF: 325 (24.5), 340 (25.2), 420 (10), 628 (9.9). Anal. Calcd for $C_{33}H_{33}N_8Fe$: C, 66.33; H, 5.57; N, 18.75. Found: C, 66.05; H, 5.5; N, 18.69.

X-Ray Crystallographic Data Collection and Refinement of the Structures. An orange single crystal of **1**, black crystals of **3** and **5**, and a deep green crystal of **4b** were coated with perfluoropolyether, picked up with nylon loops, and were immediately mounted in the nitrogen cold stream of the diffractometer to prevent loss of solvent. A Bruker-Nonius KappaCCD diffractometer equipped with a Mo-target rotating-anode X-ray source and a graphite monochromator (Mo Kα, λ = 0.71073Å) was used throughout. Final cell constants were obtained from least-squares fits of all measured reflections. Intensity data were corrected for absorption using intensities of redundant reflections. The structures were readily solved by Patterson methods and subsequent difference Fourier techniques. The Bruker ShelXTL[32] software package was used for solution, refinement and artwork of the structures. All non-hydrogen atoms were anisotropically refined and hydrogen atoms were placed at calculated positions and refined as riding atoms with isotropic displacement parameters. Crystallographic data of the compounds are listed in Table 1.

A dichloromethane and a water molecule of crystallization share a position in compound **1**. The occupation ratio refined to about 0.6:0.4. The dichloromethane molecule was refined with restrained C−Cl bond distances using the SADI instruction of ShelXL97. Two dichloromethane solvent molecules in the asymmetric unit of complex **3** were found to be disordered over two sites. The same instruction of ShelXL97 was used for the refinement of the split positions, and equal anisotropic displacement parameters were assigned to corresponding disordered atoms. The occupation factors for the two split positions refined to ratios of about 0.69:0.31 (C400 and C450) and 0.87:0.13 (C300 and C350), respectively.

The anion and acetonitrile molecules in compound **4b** were found to be severely disordered. The PF_6^- anion disorders over two positions of which one, containing P(70), is at a center of inversion. The second half of the PF_6^- anion, containing P(60), is on a general position but mixes with an acetonitrile molecule of crystallization. A number of restraints were used to support reasonable geometries of PF_6^-, and acetonitrile. P−F and F−F distances were restrained using the SADI instruction of ShelXL97. Equal anisotropic displacement parameters were given to corresponding disordered P and F atoms. The SAME and EADP instruction was used to restrain the geometrical thermal displacement parameters of disordered acetonitrile molecules, giving a total of 474 restraints.

(32) *ShelXTL*, v 6.14; Bruker AXS Inc.: Madison, WI, 2003.

Physical Measurements. ^{1}H NMR spectra were collected on a Varian Mercury 400 MHz instrument. Electronic spectra were recorded on a Perkin-Elmer double-beam photometer. Electrochemical measurements were carried out using an EG&G potentiostat/galvanostat; the working electrode was glassy carbon (CV) or Pt gauze (coulometry), the reference electrode was $Ag/AgNO_3$, and the auxiliary electrode was Pt wire. Fc^+/Fc was used as an external reference in all solutions, and all potentials are reported versus Fc^+/Fc, unless otherwise noted. Magnetic susceptibility data were recorded using a SQUID magnetometer (MPMS7, Quantum Design); 1.0 T, 2−300 K. Susceptibility data were corrected for underlying diamagnetism using tabulated Pascal's constants. X-band EPR spectra were collected on a Bruker ESP 300 spectrometer. Mössbauer data were recorded on an alternating constant-acceleration spectrometer. The minimum experimental line width was 0.24 mm s^{-1} (full width at half-height). The sample temperature was maintained constant in an Oxford Instruments Variox or an Oxford Instruments Mössbauer-Spectromag 2000 cryostat, which is a split-pair superconducting magnet system for applied fields (up to 8 T). The field at the sample is oriented perpendicular to the ç-beam. The ^{57}Co/Rh source (1.8 GBq) was positioned at room temperature inside the gap of the magnet system at a zero-field position. Isomer shifts are quoted relative to iron metal at 300 K. Data simulation was carried out using the programs "JulX" (SQUID), "EView" (EPR), and "MFIT" (Mössbauer) by E. Bill.

Calculations. Calculations were performed using the ORCA program package.[33] The geometry optimizations were carried out at the B3LYP level[34−36] of DFT. The all-electron Gaussian basis sets were those reported by the Ahlrichs group.[37,38] Triple-ζ quality basis sets (TZVP) with one set of polarization functions were used for iron, nitrogen, and oxygen atoms.[38] The carbon and hydrogen atoms were described by smaller polarized split-valence SV(P) basis sets, double-ζ quality in the valence region with a polarizing set of d-functions on the non-hydrogen atoms.[37] The self-consistent field (SCF) calculations were tightly converged (1×10^{-8} Eh in energy, 1×10^{-7} Eh in the density change, and 1×10^{-7} in the maximum element of the DIIS error vector). The geometries were considered converged after the energy change was less than 5×10^{-6} Eh, the gradient norm and maximum gradient element were smaller than 1×10^{-4} Eh/Bohr and 3×10^{-4} Eh/Bohr, respectively, and the root-mean square and maximum displacements of atoms were smaller than 2×10^{-3} Bohr and 4×10^{-3} Bohr, respectively. Corresponding orbitals[39] and density plots were generated using the program, Molekel (v 4.3). The broken symmetry (BS) approach and formalism used for several of the calculations described herein has been described previously.[40,41] The label BS(n,m) denotes n spin up electrons and m spin-down electrons. MO diagrams and spin-density plots derived from broken symmetry calculations were used only in the case where the resulting final single point energy was found to be significantly lower than for the spin unrestricted closed shell calculation (UKS).

Non-relativistic single point calculations on the optimized geometries of iron complexes with the B3LYP functional were carried out to determine the Mössbauer spectral parameters. Mössbauer calculations employed the CP(PPP) basis set[42] for iron and the TZV(P) basis sets for N and O atoms. The SV(P) basis sets were used for the remaining atoms. Mössbauer isomer shifts were calculated from the computed electron densities at the iron centers as previously described.[43]

Acknowledgment. The authors thank Professor Karl Wieghardt for support of this research and for insightful discussions. A.C. gratefully acknowledges the Spanish Ministry (MEC) for a Ph.D. grant. We thank Petra Höfer, Heike Schucht, Bernd Mienert, Frank Reikowski, and Andreas Göbels for technical assistance.

Supporting Information Available: Additional spectroscopic data, including the NMR spectra of **1** and **4**, EPR spectrum of **2**, magnetic susceptibility data for **3** and **5**, Mössbauer data for **4a**, and further electrochemical data are available as a pdf file. This material is available free of charge via the Internet at http://pubs.acs.org.

IC8020172

(33) Neese, F.; *2.6, revision 4 ed.*; Chemie, M.-P. I. f. B., Ed. Mülheim/Ruhr, Germany, 2005.
(34) Becke, A. D. *J. Chem. Phys.* **1986**, *84*, 4524.
(35) Becke, A. D. *J. Chem. Phys.* **1993**, *98*, 5648.
(36) Lee, C. T.; Yang, W. T.; Parr, R. G. *Phys. Rev. B* **1988**, *37*, 785.
(37) Schäfer, A.; Horn, H.; Ahlrichs, R. *J. Chem. Phys.* **1992**, *97*, 2571.
(38) Schäfer, A.; Huber, C.; Ahlrichs, R. *J. Chem. Phys.* **1994**, *100*, 5829.
(39) Neese, F. *J. Phys. Chem. Solids* **2004**, *65*, 781.
(40) Noodleman, L. *J. Chem. Phys.* **1981**, *74*, 5737.
(41) Noodleman, L.; Davidson, E. R. *Chem. Phys.* **1986**, *109*, 131.
(42) Neese, F. *Inorg. Chim. Acta* **2002**, *337*, 181.
(43) Sinneker, S.; Slep, L. D.; Bill, E.; Neese, F. *Inorg. Chem.* **2005**, *44*, 2245.